Supplementary Material

S1. Quasiparticles in Fabry Perot and optical-like Mach Zehnder interferometers

Fractional quantum Hall (FQH) interferometers probe bulk properties such as quasiparticle charges and statistics using edge states. Quasiparticles in the bulk are well-defined, manifesting as local finite-energy excitations with a quantized charge. In contrast, the gapless edges permit excitations of arbitrary charge. To bridge the conceptual difference, adopting a shared language to describe both bulk and edge properties is helpful.

The boundary of any fractional quantum Hall state at filling factor ν supports a charge mode, i.e., a phase field ϕ governed by the Hamiltonian, $H_{\text{edge}} = u \int dx \, (\partial_x \phi)^2$. This mode encodes the charge density on the edge via $\rho = \frac{1}{2\pi} \partial_x \phi$, in units of the electron charge. A *finite* quantum Hall droplet of electrons can only carry an integer charge. Consequently, the total charge on the edge, which is given by the winding of ϕ in units of 2π, i.e., $Q = \frac{1}{2\pi} \int dx \; \partial_x \phi$ is an integer for any ν, unless the droplet's bulk contains quasiparticles. In systems with multiple boundaries (e.g., inner and outer edges in the Corbino geometry), the total charge on all edges, $Q \equiv \sum_i Q_i$ is quantized as an integer. By contrast, the charges Q_i on individual edges can change in steps of the fundamental quasiparticle charge e^* .

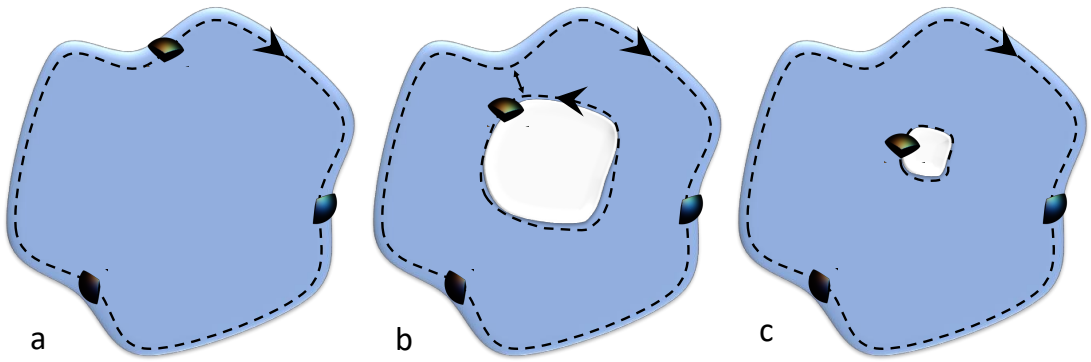

Figure S1*:* **Quasiparticles in a fractional quantum Hall droplet.** (a) The gapless edge of an FQH droplet supports arbitrarily charged excitations, provided the total charge is an integer. (b) Quasiparticles with fractional charge e^* can transfer between the inner and the outer edge, similar to a quantum point contact (QPC) (c) Shrinking the inner region to a point when the inner edge carries fractional charge results in a bulk quasiparticle.

Bulk quasiparticles can be described as edge modes encircling a small region of altered filling factor (Figure S1). Consider a small 'anti-dot' region with zero filling, much smaller than the quantum Hall droplet. This system realizes the Corbino geometry, with an outer edge mode encircling the droplet and an inner edge around the anti dot. The states on the inner edge are

subject to finite size quantization, meaning their energy levels are discrete. Varying the magnetic field, electron density, or the anti dot area continuously changes these energies. When it becomes favorable, a fractional charge e^* transfers from the droplet's outer (longer) edge to the periphery of the anti dot. The fractional charge on the inner edge is equivalent to a bulk quasiparticle. Specifically, slowly shrinking a well-isolated anti dot to a point does not change charge or statistics, which are quantized. Once the anti dot has been fully removed, a bulk quasiparticle remains.

This analysis holds even when the anti dot's filling factor is non-zero. If the anti dot realizes a fractional quantum Hall state at a filling factor ν', the total charge in its vicinity is still quantized according to the surrounding bulk. If that charge had a different fractional value, shrinking the dot to zero would leave behind a finite energy excitation with a charge not supported by the quantum Hall bulk, creating a contradiction. In terms of the edge modes, the anti-dot at filling ν' creates an additional charge mode at its perimeter. Since the anti dot only has a single (outer) boundary, this additional mode can only carry an integer charge (i.e., 2π windings), while the bulk's inner mode permits $2\pi e^*$ windings. The two combine into a total charge mode with $2\pi e^*$ windings at the perimeter of the anti-dot. Therefore, the total charge localized near the anti dot remains quantized at e^*, dictated by the surrounding bulk at filling ν. If the anti-dot supports fractional charges $e'^* \neq e^*$, the charges only exist as neutral 'quasiparticle—quasihole' pairs, which do not contribute to the braiding phase.

The central region of a Fabry Perot Interferometer (FPI) behaves similarly to an anti dot, with the outside regions of the FPI acting as the bulk. Changes in the magnetic field or area affect the number of quasiparticles (edge-mode excitations) localized along the FPI's inner periphery, as shown by the closed loops in Fig. 1(c). However, unlike in an isolated anti-dot, the edge states couple to the states extending beyond the central part of the FPI, reducing their lifetime. The introduction of localized quasiparticles with a magnetic field and their coupling to the outside modes are intrinsic properties of FPIs and require careful treatment. By contrast, these effects are absent in both the standard and the optical-like Mach Zehnder Interferometers.

In the optical-like Mach Zehnder Interferometer (OMZI), all charge modes co-propagate and do not support localized states in the central region [Fig. 1(c)]. This desirable feature comes at the cost of only displaying AB phases without anyonic braiding contributions (Fig. 2). To observe the latter; quasiparticles must be introduced through a different mechanism, such as a top gate defining an anti dot. Varying the voltage on the anti dot introduces quasiparticles, which transfer from the outer edge. Alternatively, changing the magnetic field alters the bulk filling factor and introduces quasiparticles that can either be delocalized on the outer edge or localized at the anti-dot. As a rule of thumb, localized particles are expected to appear whenever the magnetic flux through the anti-dot area changes by one flux quantum. Since this area is much smaller than the center of the interferometer, quasiparticles are introduced at a reduced rate compared to that in the FPI. Moreover, these quasiparticles are well isolated from the interfering modes.

S2. Braiding phases of Abelian quasiparticles

The statistical properties of quasiparticles in Abelian quantum Hall states orders are efficiently captured using the K-matrix formalism **[1]**. An integer-valued matrix K and a charge vector $\boldsymbol{t}$ encode a state at bulk filling factor $\nu = \boldsymbol{t}^T K^{-1} \boldsymbol{t}$, whose vacuum interface is described by the Lagrangian

$$L = \frac{1}{4\pi} \sum_{i,j} \partial_x \phi_i \left(K_{ij} \partial_t \phi_j - V_{ij} \partial_x \phi_j \right),$$

with a non-universal velocity matrix V. All bulk quasiparticles of the topological order $(K, \boldsymbol{t})$ are specified by integer vectors $\boldsymbol{l}$ with the electric charge given by

$$Q(\boldsymbol{l}) = \boldsymbol{t}^T K^{-1} \boldsymbol{l}. \quad (1)$$

Fully encircling one quasiparticle defined by $\boldsymbol{l_1}$ by another defined by $\boldsymbol{l_2}$ yields the braiding phase

$$\theta(\boldsymbol{l_1}, \boldsymbol{l_2}) = 2\pi \, \boldsymbol{l_1}^T K^{-1} \boldsymbol{l_2}. \quad (2)$$

For Jain states at $\nu = \frac{n}{2pn+1}$, K is an $n \times n$ matrix, which can be expressed using the identity matrix and matrix of ones as

$$K = \begin{pmatrix} 1 & \cdots & 0 \\ \vdots & \ddots & \vdots \\ 0 & \cdots & 1 \end{pmatrix} + 2p \begin{pmatrix} 1 & \cdots & 1 \\ \vdots & \ddots & \vdots \\ 1 & \cdots & 1 \end{pmatrix}, \quad (3)$$

with n −component charge vector $\boldsymbol{t} = (1, \ldots, 1)$. Inverting Eq. (3) yields

$$K^{-1} = \begin{pmatrix} 1 & \cdots & 0 \\ \vdots & \ddots & \vdots \\ 0 & \cdots & 1 \end{pmatrix} - \frac{2p}{1+2np} \begin{pmatrix} 1 & \cdots & 1 \\ \vdots & \ddots & \vdots \\ 1 & \cdots & 1 \end{pmatrix}. \quad (4)$$

For a fundamental quasiparticle $\boldsymbol{l_0} = (1,0,0, \ldots)$, Eqs. (1) and (2) yield the known results for Jain states,

$$Q(\boldsymbol{l_0}) = \frac{1}{1+2np},$$

$$\theta(\boldsymbol{l_0}, \boldsymbol{l_0}) = 2\pi - 2\pi \frac{2p}{1+2np}.$$

[1] *Quantum Field Theory of Many-body Systems*, Xiao-Gang Wen (Oxford Graduate Text, 2004)

For the first Jain's states, $p = 1$. Ignoring the first 2π term, the reduced phase is: $\frac{\theta^*}{2\pi} = \frac{2}{1+2n}$ (see above).

ν	n	theory: $\frac{\theta^*}{2\pi} \bmod 1$	$\frac{\theta^*}{2\pi}$, from $B - V_{MG}$	$\frac{\theta^*}{2\pi}$, from $B - V_{TG}$
$1/3$	1	$-\frac{1}{3} = -0.33$	-0.35 ± 0.11	-0.38
$2/5$	2	$\frac{2}{5} = 0.40$	-0.39 ± 0.05	-0.42
$3/7$	3	$\frac{2}{7} = 0.29$	$\pm 0.35 \pm 0.05$	–

Table 1. Comparison of the theoretically expected value $\frac{\theta^*}{2\pi} = \frac{2}{1+2n}$ for the first three Jain fillings. Spatial lock-in method calculation of the 'pajamas' in Fig. 3 ($B - V_{MG}$), the average of the phase jumps is taken in the convention that all the phase jumps are in the range between $-\pi$ and π ; direct phase jumps from the B dependence across the top gate abrupt ΔV_{TG} change in Fig. 4 ($B - V_{TG}$).

S3. Phase slips analysis by spatial *lock-in method*

The main interference signal in the space of B and V_{MG} (and V_{TG}) is a periodic signal that can be described by:

$$T(\mathbf{r}) = A(\mathbf{r})\sin(\mathbf{qr} + \theta(\mathbf{r})), \qquad (1)$$

where $\mathbf{q} = (q_B, q_V)$ is the frequency of the Aharonov-Bohm oscillations, $\mathbf{r} = (B, V)$, and $\theta(\mathbf{r})$ is the additional phase that remains constant in the absence of the phase slips and increases stepwise after each phase slip by the value of the statistical phase, $\mathbf{r} = (B, V)$.

To extract the statistical phase term $\theta(\boldsymbol{r})$, we define the *lock-in signal*,

$$s_1(\mathbf{r}) = \cos(\mathbf{qr}) \qquad (2)$$
$$s_2(\mathbf{r}) = \sin(\mathbf{qr}),$$

multiplying the original signal $T(\boldsymbol{r})$ by s_1 and s_2 separately,

$$s_1(\mathbf{r}) \times T(\mathbf{r}) = A(\mathbf{r})\cos(\mathbf{qr})\sin\big(\mathbf{qr} + \theta(\mathbf{r})\big) \tag{3}$$

$$= \frac{A(\mathbf{r})}{2}(\sin(\mathbf{qr} + \mathbf{qr} + \theta) + \sin(\mathbf{qr} + \theta - \mathbf{qr}))$$

$$= \frac{A(\mathbf{r})}{2}(\sin(2\mathbf{qr} + \theta(\mathbf{r})) + \sin\theta(\mathbf{r}))$$

$$s_2(\mathbf{r}) \times T(\mathbf{r}) = A(\mathbf{r})\sin(\mathbf{qr})\sin\big(\mathbf{qr} + \theta(\mathbf{r})\big)$$

$$= \frac{A(\mathbf{r})}{2}(\cos(\mathbf{qr} + \theta(\mathbf{r}) - \mathbf{qr}) - \cos(\mathbf{qr} + \theta(\mathbf{r}) + \mathbf{qr}))$$

$$= \frac{A(\mathbf{r})}{2}\ (\cos\theta(\mathbf{r}) - \cos(2\mathbf{qr} + \theta(\mathbf{r})))$$

Finally, we add low-pass filtering (LPF) to the 'new signals',

$$LPF(s_1(\mathbf{r}) \times T(\mathbf{r})) = \frac{A(\mathrm{r})}{2}\sin\theta(\mathbf{r}) \tag{4}$$

$$LPF(s_2(\mathbf{r}) \times T(\mathbf{r})) = \frac{A(\mathbf{r})}{2}\cos\theta(\mathbf{r})$$

$$\frac{LPF\big(s_1(\mathbf{r}) \times T(\mathbf{r})\big)}{LPF\big(s_2(\mathbf{r}) \times T(\mathbf{r})\big)} = \tan\theta(\mathbf{r}) \tag{4}$$

$$\theta(\mathbf{r}) = \arctan\frac{LPF(s_1\ (\mathbf{r}) \times T(\mathbf{r}))}{LPF(s_2\ (\mathbf{r}) \times T(\mathbf{r}))}$$

In the figures below, a step-by-step illustration of the method is provided.

Step 1. Raw data of pajamas with phase slips (**Fig. 1**),

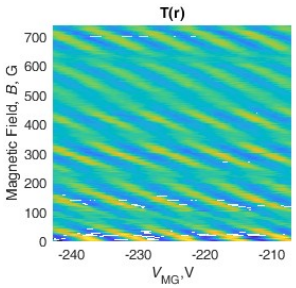

Fig. 1

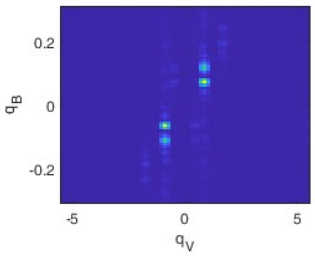

Fig. 2

Step 2. Performing a *fast Fourier transform* to determine the spatial frequency **q** (**Fig. 2**)

Since the frequency q_B is not a single sharp peak, the frequency $\mathbf{q}$ used in the analysis is defined by choosing a frequency between the two visible peaks that best reflects the stepwise behavior of $\theta(\mathbf{r})$.

Step 3. Multiplication by s_1 and s_2

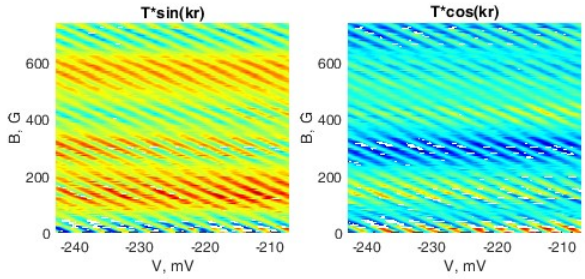

Step 4. Low-pass filtering

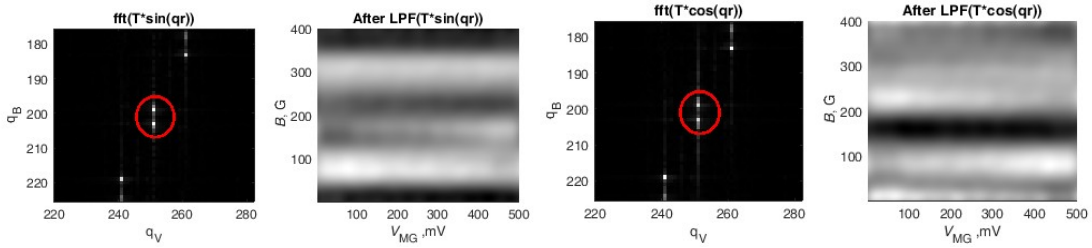

Step 5: Color plot of the $\theta(B, V_{mg})$

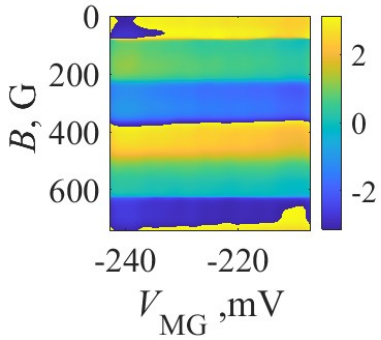

Step 6: Averaging in a range of voltages $V_1 < V < V_2$ (table 2).

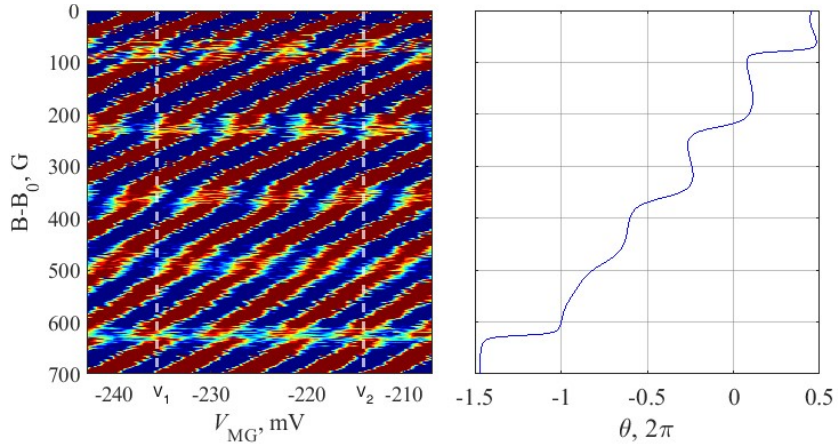

V_{MG}, mV	$1/3$	$2/5$	$3/7$
V_1, mV	-106.2	-235.6	-465.0
V_2, mV	-105.0	-214.2	-455.3

Table 2. Voltage range for averaging the phase to get the result in Fig. 3 from the main text.

The spatial lock-in method is advantageous since it allows isolating of the phase slips associated with the specific frequency of Aharonov Bohm oscillations. It effectively captures the absolute value of each phase slip at the chosen frequency. It is less reliable for capturing the direction of the phase slip since the visibility during the phase jumps is significantly suppressed. In addition, the Aharonov-Bohm frequency along the wide range of the magnetic field can be subject to slight change, which may lead to an error in defining the phase flip size.

An alternative method is to use a fast Fourier transform for each horizontal slice (fixed magnetic field) and look at the evolution of the complex phase along the magnetic field. This method might more accurately detect the frequency change along *B* axis. However, a linear correction is required to determine the phase slip, which is unnecessary in the abovementioned method.

S4. Interfacing Abelian fractional states

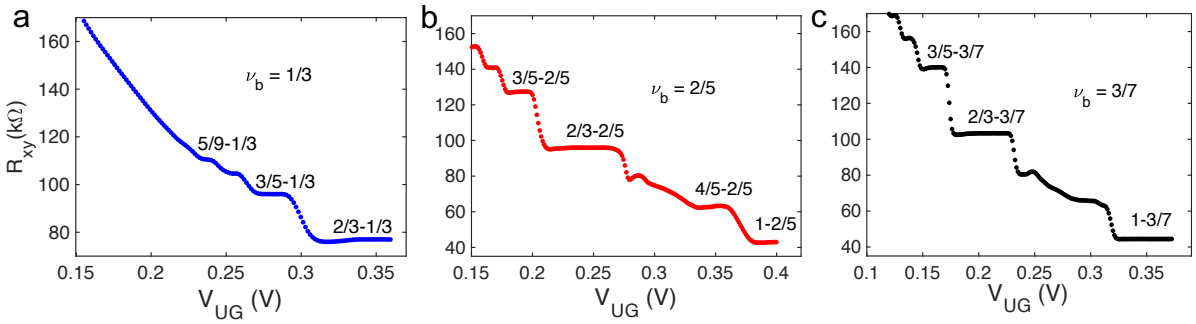

Figure S2: **Interfacing Abelian fractional states**. Two terminal resistance measurements at the interface between $\nu_u - \nu_b$. The bulk is fixed at $\nu_b = 1/3$, 2/5, 3/7, and the upper gate (UG) is swept with positive bias. Clear quantized plateaus corresponding to ν_u= 5/9, 4/7, 3/5 and 2/3 (a) ν_u= 3/5, 2/3,4/5 and 1 (b) ν_u= 3/5, 2/3, and 1 (c); accurate to ~1% are observed. For $\nu_b = 2/5$, ν_u=1 corresponds to a 150% increase in the 2DEG density underneath the gate. After the charge has equilibrated, the $'\nu_u - \nu_b'$ interface charge mode is accompanied by upstream neutral modes.

S5: Interference of counter-propagating edge modes

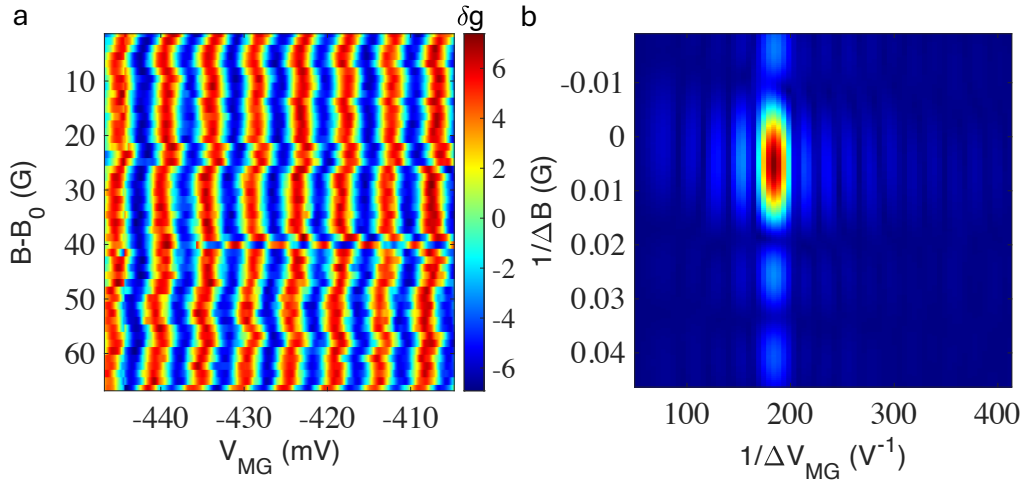

Figure S3: **Interference in Fabry-Perot interferometer at ν=1/3.** (a) Transmission oscillation of the edge mode at ν=1/3 in the 0-1/3-0 configuration. While the transmission is independent of the magnetic field B, it oscillates as a function of V_{MG}. This is a typical behavior of Coulomb-dominated (CD) interference. (b) 2D FFT gives the periodicity ΔV_{MG}=5.5 mV.

S6: Dependence of flux periodicity on the interface edge mode on the population side

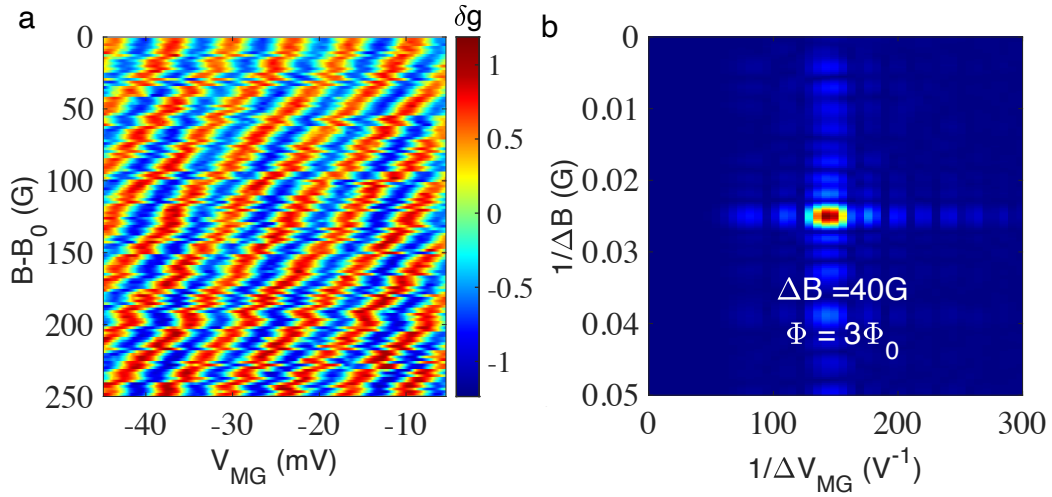

Figure S4: **Aharonov Bohm pajama in optical-like MZI at ν=1/3** (a) Conductance oscillation with the interfering 1/3 edge mode in the B-V_{MG} plane in the filling-factor configuration fillings: 5/9 - 1/3 -0. The top gate is fixed at V_{TG}=0 V. As anticipated, the pajama is free from phase flips. (b) 2D Fourier transforms of the pajamas plots showing a single peak. The periodicity in B is 40G and in V_{MG} is 7mV. The estimated AB area is $\sim$ 3 μm^2, leading to a flux periodicity $3\Phi_0$.

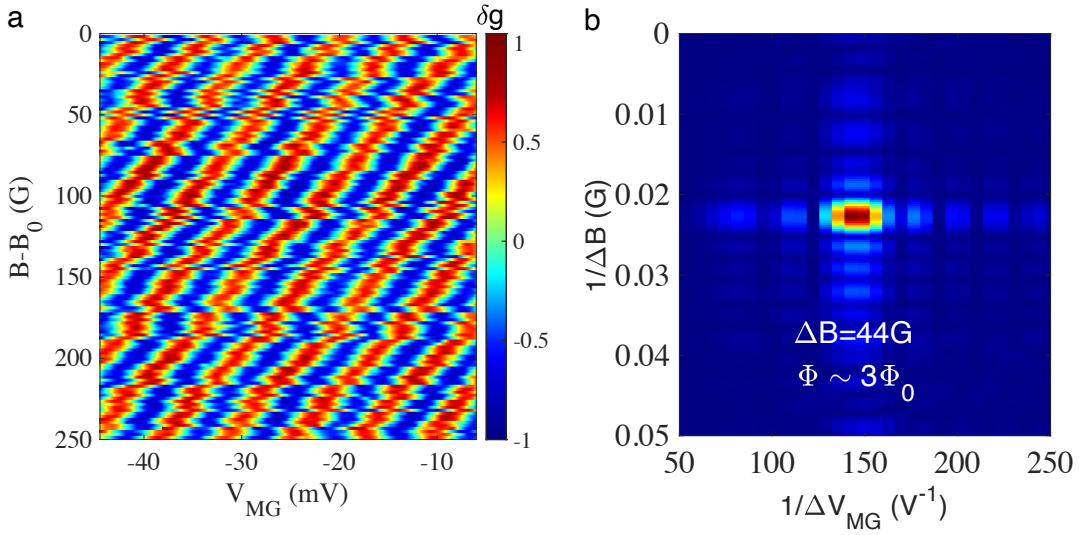

Figure S5: **Aharonov Bohm pajama in optical like MZI at ν=1/3** (a) Transmission oscillation with the interfering 1/3 edge mode in the B-V_{MG} plane with a 3/5-1/3-0 configuration. The top gate (of the anti dot) is fixed at V_{TG}=0 V. The Pajama is free of phase jump. (b) 2D Fourier transforms of the pajama plot showing a single peak. The periodicity in B is 44G and V_{MG} is 6.8mV. The calculated AB area is $\sim$ 2.82 μm^2, leading to a flux periodicity $\sim 3\Phi_0$. Similar results were observed in '2/3-1/3-0' (see main text), and '5/9-1/3-0' (Figure S4) and for an outer partitioned 1/3 mode in the '1-2/5-0' configuration (Figure S7), suggesting flux periodicity is solely determined by the QPC filling and independent of ν_u.

S7: Interference of outer edge modes in an optical-like MZI

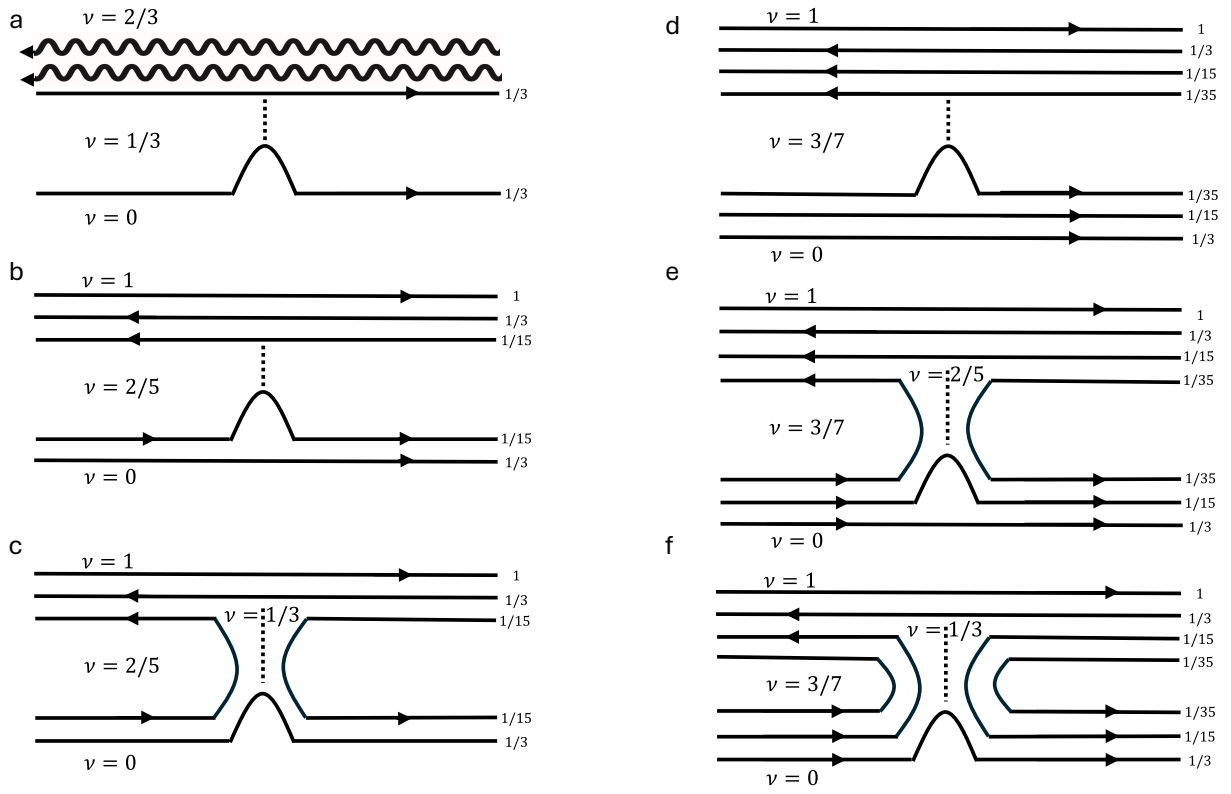

Figure S6: **Edge mode partitioning in the co-propagating QPC.** The filling factor inside the QPC determines the Aharonov Bohm flux periodicity and the statistical phase slip in the respective interferometer. The solid lines are charged modes and the wavy lines are neutral modes. (a) Partitioning the $1/3$ mode: $\nu_{\mathrm{bulk}} = 1/3$, $\nu_{\mathrm{qpc}} = 1/3$ (b) Partitioning the inner $1/15$ mode: $\nu_{\mathrm{bulk}} = 2/5$, $\nu_{\mathrm{qpc}} = 2/5$ (c) Partitioning the outer $1/3$ mode: $\nu_{\mathrm{bulk}} = 2/5$, $\nu_{\mathrm{qpc}} = 1/3$ (d) Partitioning the inner $1/35$ mode: $\nu_{\mathrm{bulk}} = 3/7$, $\nu_{\mathrm{qpc}} = 3/7$ (e) Partitioning the middle $1/15$ mode: $\nu_{\mathrm{bulk}} = 3/7$, $\nu_{\mathrm{qpc}} = 2/5$ (f) Partitioning the outer $1/3$ mode: $\nu_{\mathrm{bulk}} = 3/7$, $\nu_{\mathrm{qpc}} = 1/3$.

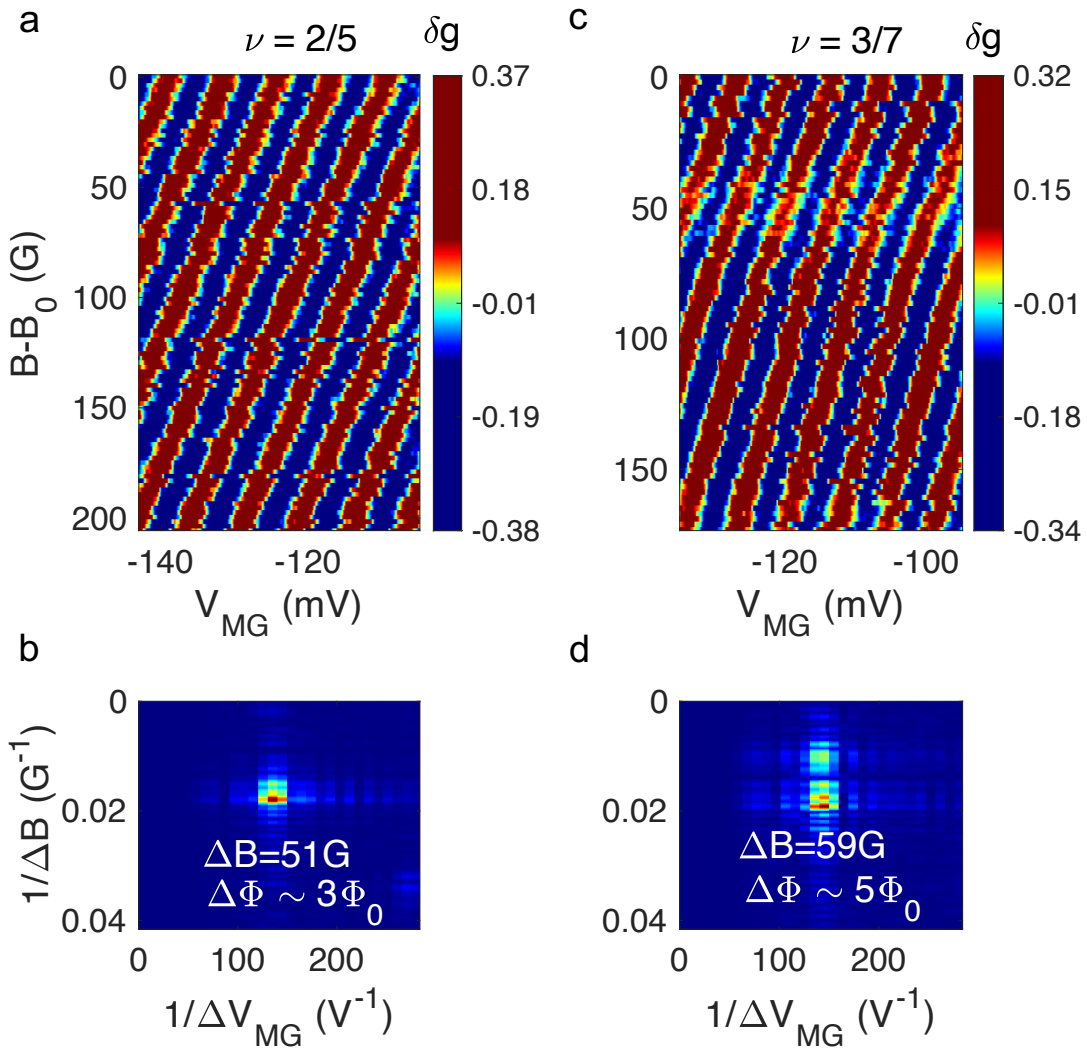

Figure S7: **Aharonov Bohm pajamas of the co-propagating outer edge mode for the bulk filling ν_u=2/5 and ν_u=3/7.** For these measurements, the QPCs are biased to achieve 90% transmission of the outer 1/3 mode (or the 1/15 mode) of the bulk with filling factor 2/5 (or 3/7). Top gate (TG) is kept at V_{TG}=0V. Within the tolerable voltage limit of the QPCs, we could not partition the outer 1/3 mode of the ν=3/7 bulk. The color scale shows conductance oscillation with clear periodicities corresponding to different QPC filling: $3\Phi_0$ (a,b) and $5\Phi_0$ (c,d). The estimated AB area for the outer mode of ν=2/5 is ~2.45 μm^2, and for the middle edge of ν=3/7 is ~ 3.5 μm^2. As explained in the main text, the small area correction depends on the pinching voltage of the QPC.

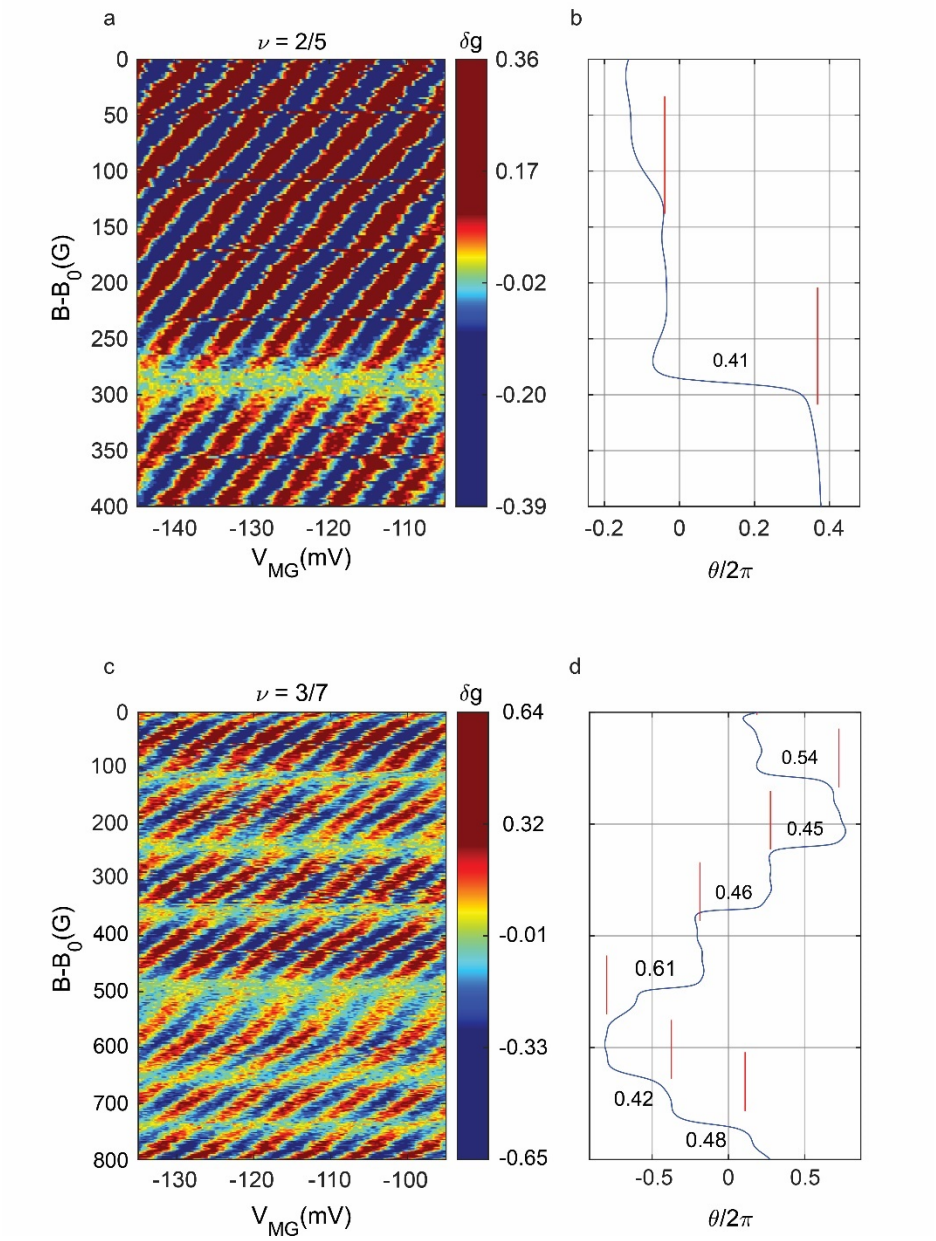

Figure S8: **Aharonov Bohm pajamas with phase slips of the co-propagating outer edge mode in the bulk filling ν_u=2/5 and 3/7.** The conductance oscillation as a function of B and modulation gate voltage V_{MG} show Aharonov Bohm interference with clear phase jumps. For these measurements, the QPCs are biased to achieve 90% transmission of the bulk filling's outer 1/3 mode (a) (or middle 1/15 mode (c)) of 2/5 (or 3/7). The top gate voltage V_{TG} is tuned to -50mV to -90mV, far from complete depletion under the gate. The discrete phase jumps are similar to those observed for the corresponding innermost modes. Figures **b, and d** present the calculated phase slips with the Lock-In technique (see **Methods** and **S3**). The red lines indicate the regions of a constant phase.